Research Article | Vol. 12, No. 2 / 1 February 2021 / Biomedical Optics Express 1123
Biomedical Optics EXPRESS

Fiber-based SORS-SERDS system and chemometrics for the diagnostics and therapy monitoring of psoriasis inflammatory disease *in vivo*

JOHANNES SCHLEUSENER,[1,4,5] SHUXIA GUO,[2,3,4] MAXIM E. DARVIN,[1] GISELA THIEDE,[1] OLGA CHERNAVSKAIA,[3] FLORIAN KNORR,[3] JÜRGEN LADEMANN,[1] JÜRGEN POPP,[2,3] AND THOMAS W. BOCKLITZ[2,3,6]

[1]*Center of Experimental and Applied Cutaneous Physiology, Department of Dermatology, Venerology and Allergology, Charité – Universitätsmedizin Berlin, Humboldt-Universität zu Berlin, Berlin Institute of Health, Charitéplatz 1, 10117, Berlin, Germany*
[2]*Institute of Physical Chemistry and Abbe Center of Photonics, Friedrich Schiller University of Jena, Helmholtzweg 4, 07743 Jena, Germany*
[3]*Leibniz Institute of Photonic Technology, Albert-Einstein-Straße 9, 07745 Jena, Germany*
[4]*Both authors contributed equally to this work*
[5]*Correspondence regarding medical questions should be sent to johannes.schleusener@charite.de*
[6]*Correspondence for technical issues should be sent to thomas.bocklitz@uni-jena.de*

Abstract: Psoriasis is considered a widespread dermatological disease that can strongly affect the quality of life. Currently, the treatment is continued until the skin surface appears clinically healed. However, lesions appearing normal may contain modifications in deeper layers. To terminate the treatment too early can highly increase the risk of relapses. Therefore, techniques are needed for a better knowledge of the treatment process, especially to detect the lesion modifications in deeper layers. In this study, we developed a fiber-based SORS-SERDS system in combination with machine learning algorithms to non-invasively determine the treatment efficiency of psoriasis. The system was designed to acquire Raman spectra from three different depths into the skin, which provide rich information about the skin modifications in deeper layers. This way, it is expected to prevent the occurrence of relapses in case of a too short treatment. The method was verified with a study of 24 patients upon their two visits: the data is acquired at the beginning of a standard treatment (visit 1) and four months afterwards (visit 2). A mean sensitivity of ≥85% was achieved to distinguish psoriasis from normal skin at visit 1. At visit 2, where the patients were healed according to the clinical appearance, the mean sensitivity was ≈65%.

1. Introduction

Psoriasis is a chronic inflammatory disease related to autoimmune reactions, characterized by acanthosis with disturbed keratinocyte differentiation. The pathogenesis of psoriasis is influenced by the tumor necrosis factor α, dendritic cells, and T-cells [1,2]. The prevalence of psoriasis is 0.6–4.8% in the general population [3], and is therefore considered a widespread disease that shows strong influence on the quality of life [4,5]. There is currently no cure for psoriasis, only the symptoms, mainly inflammation, are treated with different medications including corticosteroids, and also biologicals. An acute treatment of psoriasis with corticosteroids is accompanied with strong side effects as the natural cortisol production can increase the risk of infections. Side effects of other medications can reduce the DNA replication. In addition, these symptoms, if reoccurring, often require a life-long medication. The treatment of psoriasis is commonly

#413922 https://doi.org/10.1364/BOE.413922
Journal © 2021 Received 2 Nov 2020; revised 8 Jan 2021; accepted 11 Jan 2021; published 28 Jan 2021

Biomedical Optics EXPRESS

conducted until the skin surface appears clinically healed. However, at this stage, modifications in the deeper skin layers are still present. It has also been shown, that vascular modifications in the skin also precede acute psoriatic lesions [6]. If the treatment is successful, the lesions can heal without any scarring [7,8] and return to a clinically normal appearing skin [9,10], although alterations can persist in the treated skin sites. For instance, it has been found that $CD8^+$ T-cells remain present and the LYVE-1 gene was persistently downregulated in clinically healed psoriasis skin [8].

The severity of psoriasis lesions and its transformation during the healing process can be qualitatively assessed by the psoriasis area and severity index (PASI), which is widely used to assess the severity (thickness, redness, and scaliness) of lesions. The PASI score is a subjective, non-reproducible parameter. It describes only the overall condition of a patient and is thus not lesion specific. Several adaptations, such as cPcASI or local PASI exist. Nonetheless, none of these indices are able to identify modifications present in deep skin layers. Using *in vivo* laser scanning microscopy, pathologic differences were observed in the papillary dermis with ≈100 µm depth for ≈50% of the psoriasis lesions appearing clinically healed on the skin surface. These pathologic modifications include changes in the papillary structure, as well as in capillary diameters (p=0.001) within the papillae [11,12]. While in normal skin, the papillae contain a single capillary loop, the papillaries in psoriasis were elongated, widened and tortuous. Also, the morphology and gene expression of lymphatic vessels remains changed in healed psoriasis lesions, clinically appearing normal [8]. Terminating treatment at this point risks highly of a reoccurrence within the following 12 months, which can be significantly reduced if the treatment will be continued until no pathologic changes are detected [8]. The occurrence of relapses within the following 12 months was significantly reduced, if no pathologic changes could be detected any more [12].

Methods are needed to measure psoriasis-related biologic markers in order to objectively determine the healing process, for example, the increase of stratum corneum (SC) thickness [13], the molecular composition and the lipid structure [14]. Further, psoriasis often impairs the skin barrier function, entailing a reduced hydration status and dry skin [15]. Acute lesions are composed of parakeratotic cells, which can be assessed by histopathology. The latter is yet not perfectly suitable as a treatment monitoring method, in which measurements should be performed non-invasively and *in vivo*. Using multiphoton coherent anti-stokes Raman-scattering (CARS) tomography [16], it was further possible to detect differences in the cellular morphology and lipid concentration in a depth of 100 µm in case of inflammatory disruptions [17]. However, imaging techniques like multiphoton tomography and laser scanning microscopy, require the application and interpretation by trained personnel and do not provide objective results.

As a non-destructive method, Raman spectroscopy (RS) is particularly suitable for *in vivo* investigations. It has been particularly applied to detect molecular differences in the skin, e.g. for the detection of skin cancer [18–23]. In combination with chemometric methods [24,25], RS was shown able to detect concentration changes in skin components, such as water, keratin, natural moisturizing factors (NMF), ceramide, cholesterol, urea lactic- and trans-urocanic acid [26]. It has also been applied *in vivo* to analyze the organization of intercellular lipids [27], the folding structure of keratin [28], the hydration status based on the hydrogen bonding state of water molecules [29], the concentration of DNA [30] and the concentration and aggregation of the carotenoids [31,32]. Despite RS is mainly limited for investigation of the SC, it is also possible to apply RS for analysis of the skin until depths of papillary dermis [33–35]. Thus, by providing rich molecular information of skin composition, RS is believed highly potential for objective psoriasis detection. In fact, applications of RS in relation to psoriasis have been reported with promising findings. The intensity of the Raman band at 1418 cm^{-1} was found to decrease in psoriasis biopsies, which was assumed to be associated to the NMF concentration

Biomedical Optics EXPRESS

[36]. It was therefore suggested to combine the relative NMF concentration with established markers of the secondary protein structure and lipid organization for treatment monitoring [37].

Further, a de-lipidation in the SC has been found, indicating a reduced barrier function due to hyperkeratotic activity [38]. Similarly, decreased lipid organization in the SC was found [39]. In addition, Raman bands were found to shift towards higher wavenumbers in psoriasis skin compared to normal skin. For instance, the shift of the CH_2 Raman band around 2850 cm^{-1} towards higher wavenumbers in psoriatic skin [1] is directly related to an increase of hexagonal lipid organization in the SC, i.e. reduced skin barrier function [40]. The shift of Raman band positions of Amide I around 1650 cm^{-1} and the CH_3 around 2930 cm^{-1} in psoriatic skin [41] is related to changes of keratin folding and the possibility to bind water molecules in the SC [28].

Apart from the capability of delivering molecular fingerprints, RS has seen huge development in *in vivo* detection thanks to fiber-based systems. It becomes possible to measure body sites that are conventionally difficult to access [26,42–44]. For instance, *in vivo* discrimination of skin cancer has been achieved in several groups using fiber-based RS [18,20,45]. RS is clearly a promising approach in psoriasis diagnosis. However, it is not without challenges, such as intensity variations due to bending losses [46]. Fiber probes usually record an integrated signal from larger sampling volumes with a low spatial resolution compared to the application by confocal microscopes [42]. The origin of the majority of the detected signal can however be influenced by changing parameters, such as the excitation wavelength and the spot diameters, numerical apertures, as well as source–detector distances of excitation and detection fibers. Appropriate fiber probe geometries were modeled using Monte Carlo simulations [47]. By using multiple source–detector distances in a single fiber probe, depth dependent Raman spectra can be recorded, which has been termed spatially offset Raman spectroscopy (SORS) [48,49].

Another major issue of applying RS comes to the strong autofluorescence from skin and/or optical materials, especially in the fingerprint range [50], which bleach over time [34]. Such fluorescence background may be reduced, for example, by using a near-infrared excitation or choosing appropriate optical filters, but cannot be completely eliminated. 785 nm is frequently used as an excitation wavelength, as it manifests a good compromise of low fluorescence background, yet sufficiently high Raman cross section, which decreases with increasing wavelength, high penetration depth in skin and detector sensitivity [51]. Most biological molecules, such as tryptophan, collagen, elastin, FAD, NADH/NAD+ do not fluoresce under near-infrared excitation [52–54], melanin in the skin does [55–57]. Recording Raman spectra only in the high wavenumber region can reduce the fluorescence background, entailing simpler fiber probe designs, but in this case molecular information present in the fingerprint is lost [50,58]. Time-gating has been applied in order to block the fluorescent component, which has a long lifetime compared to the nearly instantaneous Raman effect [59,60]. Modulated Raman spectroscopy has been applied [61,62]. Specially designed fiber probes comprising hollow core fibers were also used, but these fibers are usually very sensitive to bending losses [63,64]. A more commonly applied approach is the mathematical baseline correction, which, however, can fail if the fluorescence is too dominating. Another option is shifted-excitation Raman difference spectroscopy (SERDS), in which two spectra are acquired at two slightly different excitation wavelengths ($\approx$1 nm). The Raman bands shift according to the excitation, but the fluorescence stays almost identical according to Kasha's rule [65]. It is thus possible to obtain a fluorescence-free difference spectrum from the two recorded spectra [66,67]. Noteworthy, the advantage of SERDS-SORS to tackling high fluorescence as well as enabling sub-surface analysis has been reported elsewhere [68].

The aim of this study was to evaluate fiber probe-based SORS-SERDS system as an objective non-invasive *in vivo* detection method for monitoring the healing process of psoriasis. If successful, this method could be applied to optimize the treatment period in order to reduce the occurrence of relapses. This exploratory clinical study was conducted according to the German implementation of the Medical Device Directive 93/42/EWG (MPG). *In vivo* measurements

Biomedical Optics EXPRESS

were performed on 30 patients suffering from acute psoriatic inflammatory skin lesions at the beginning (visit 1) and four months after the beginning of the treatment (visit 2), when the acute psoriatic inflammatory skin lesions were usually healed.

2. Materials and methods

2.1. Study protocol

The study included 30 Patients (14 female, 16 male) of skin type I–III (Fitzpatrick classification [69]) with acute psoriatic lesions between November 2017 and July 2019. Six of these patients (4 female and 2 male) did not conclude the study. Two participants could no longer be reached and three participants could not manage to attend visit 2, which was due four months after the beginning of the standard treatment (visit 1). For one participant, the final diagnose turned out not to be psoriasis. The experiments were conducted in the Department of Dermatology, Venerology and Allergology, Charité – Universitätsmedizin Berlin, Germany. The patients were aged between 32 and 82 years (mean 56 ± 17). The measurements were performed on five positions of a psoriatic lesion of size ≥ 1 cm^2 that did not have flakes and five positions from clinically normal skin close to the lesion. Before the measurements, the skin was washed with cold running water and a washing lotion (Lifosan soft, B. Braun Melsungen AG, Melsungen, Germany), if necessary in case of remaining ointment. A hair removal was not necessary. Each patient was measured twice: at the beginning of a standard inpatient treatment (visit 1) and four months after the beginning of this treatment, when the acute lesions were usually healed (visit 2). This was chosen, due to the varying healing process and accordingly varying lengths of treatment. In particular, the lesions under measurement were photographed, schematically recorded in the case report file and the measurement positions were copied to a transparent foil, covering the lesions, along with static landmarks like naevi. The foil was well stored and served as a stencil to recover the exact measurement positions for the measurements on visit 2 (Fig. 1). The clinical assessment if lesions were psoriasis was conducted according to the PASI criteria redness, thickness and desquamation by a dermatologist.

Fig. 1. Arm of a patient with marked psoriatic lesions and normal skin for control at visit 1 (left), with copied measurement positions on transparent foil at visit 1 (center) and at visit 2, when the lesions were mostly healed (right).

This open, controlled, non-randomized proof-of-principle study was conducted according to the declaration of Helsinki, as revised in 2013. All patients were well informed and declared a written consent for the participation. The experiments were approved by the ethics committee

Biomedical Optics EXPRESS

of Berlin and registered with the federal institute for drugs and medical devices (Eudamed-Nr. CIV-17-01-018264).

2.2. Raman spectroscopy

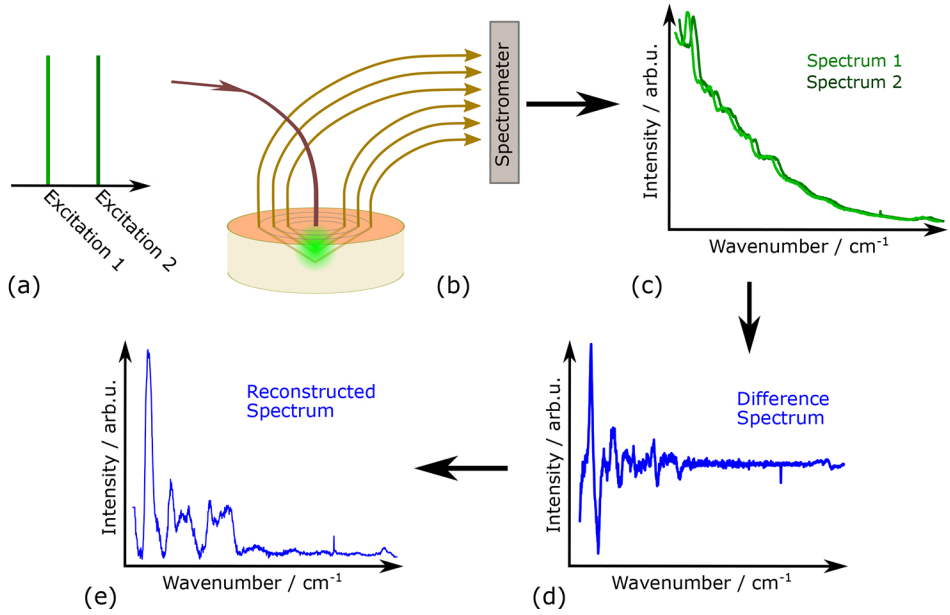

Fig. 2. Protocol of the measurement system. Raman spectra of two excitation wavelengths (a), shifted by ±0.5 nm were acquired from the skin. The collection fibers were arranged in concentric circles around the excitation to allow the detection of three source–detector distances (b). Raman difference spectra were calculated from the spectra of shifted excitation (c–d). The Raman spectra with removed fluorescence background were reconstructed from the SERDS spectra (e). The fiber-based probe design for the SORS measurements is presented in Fig. S3.

The protocol of the measurement is shown in Fig. 2. The measurement was done using two slightly different excitation wavelengths at 784.5 and 785.5 nm (approx. 8 cm^{-1}) with a continuous wave optical power of ≤20 mW using a tunable diode laser (Toptica Photonics, Graefelfing, Germany). The applied laser radiation on the skin is classified as class 1M according to DIN EN 60825. The measurement device fulfilled the demands of a medical device according to 93/42/EWG. The fiber-based probe designed for the SORS measurement was composed of a central excitation fiber (200 µm core diameter, NA=0.22) surrounded by three hexagonal shaped rings of collection fibers with source – detector distances of 245, 490 and 735 µm. The sketch of the fiber probe is shown in Fig S3. The fiber collection bundle on the spectrometer side had a linear array shape where fibers 1–6 belong to the inner, 7–18 to the middle and 19–36 to the outer ring. To filter out residual laser light and to focus the fiber end faces in the entrance slit plane of the spectrometer, an optical relay system was mounted to the spectrometer body. During measurements spectra from all rings were recorded simultaneous for each wavelength by binning the CCD detector into three sections that corresponded to the rings. The geometries of the fiber probe were modeled using Monte Carlo simulations [47,70] in order to minimize the influence from the variations in the excitation wavelength, the spot diameters, and the numerical apertures. The Monte Carlo simulations could be also used to determine the origin of the respective signals within the three rings (see Fig. S2). With different distances to the excitation fiber, the collection

Biomedical Optics EXPRESS

fibers could acquire Raman signals coming from different depths within the skin. In this way, six spectra at each position corresponding to the three depths by varying source–detector distances and two excitation wavelengths, in order to calculate SERDS spectra, were obtained. The acquisition time at each of the 10 positions was 20 s (10 s for each excitation wavelength). Each of the two spectra from the same depth but from different excitation wavelengths were used to reconstruct a fluorescence-free Raman spectrum. In the end the three reconstructed Raman spectra were appended into one spectrum for further analysis. As a detection system, a Shamrock 303i Czerny-Turner spectrometer with a DU420A-BEX2-DD back-illuminated CCD detector (Andor Technology Ltd, Belfast, Northern Ireland) was used and Raman spectra in the 675–1750 cm^{-1} wavenumber range were recorded. Control of the components and data acquisition was realized by an in-house written software based on LabVIEW (National Instruments, Austin, TX, USA).

2.3. Data analysis

All analysis was performed using an in-house written script with R language [71]. The procedures are summarized as following. All spectra were subject to a pre-processing pipeline including de-spiking, wavenumber calibration, fluorescence removal, and intensity normalization [72]. As the first step, the cosmic spikes were removed, if necessary, using an in-house script based on second-order derivative algorithm. The wavenumber axis was calibrated based on the spectra of the standard material 4-acetamedophenal [73]. Thereafter, an NNLS-based SERDS reconstruction was performed for every two spectra of the same position and depth but measured at different excitation wavelengths [74]. This resulted in three spectra for each measurement position, featuring different depths within the skin. Additionally, a baseline correction was performed on each spectrum to further remove the fluorescence baseline [75]. The three spectra from the same position were appended into one single spectrum after vector normalization *(i.e.*, $I^n(\omega_i) = \frac{I(\omega_i)}{||I(\omega)||}$*)*. This low-level data fusion enables to combine the information from the three layers of different depth and hence the classification can be done based on the information contained in all three depth levels.

The preprocessed spectra were used for classification to distinguish the normal against the psoriasis spectra. This was done based on a principal component analysis (PCA, from R package 'stats' [71]) in combination to a linear discriminant analysis (LDA, from R package 'MASS' [76]). In particular, the model was built on the spectra from the first visit. The spectra from the second visit were used only for prediction. The reason is the following. The patients may have recovered from psoriasis or were on the way of recovery at their second visit. This introduced additional variance and ambiguity to the ground-truth annotation of the samples at the second visit, making these samples problematic to be used as training data. The classification was conducted based on a leave-one-patient-out cross-validation. That is to say, spectra of each patient (both visits, five spectra of each visit) were predicted once by the model built on the spectra of the other patients at the first visit. This led to five predictions of each patient at each visit, which will be referred as 'spectra-level prediction' henceforth. Thereafter, we obtained 'patient-level prediction' through a majority vote among the predictions from the five spectra of the same patient and assign the patient as psoriasis if 3 or more spectra were predicted as 'psoriasis'. We utilized the mean sensitivity (given in Eq. (1)) as characteristics of the model quality, which is scaled between 0 and 1.

$$\text{sensitivity} = \frac{tp}{tp + fn} \tag{1.a}$$

$$\text{specificity} = \frac{tn}{tn + fp} \tag{1.b}$$

$$\text{mean sensitivity} = \frac{\text{sensitivity} + \text{specificity}}{2} \tag{1.c}$$

Biomedical Optics EXPRESS

3. Results and discussion

Figure 3 shows the mean spectra of the two visits (V1, V2) from all patients. The data from different depths within the skin were shown as depth-1, -2, and -3, respectively. Based on the results of the Monte-Carlo simulation [47], the first depth (50–150 μm) contains a majority of information of the most superficial skin areas, such as epidermis and papillary dermis. The second depth captures a majority of the signal of 150–250 μm under the skin, which corresponds to the papillary and reticular dermis. The third depth is mostly related to the skin areas deeper than 250 μm, i.e. the reticular dermis. The spectral differences between the normal and psoriasis skin were visible at the first visit but almost disappeared at the second visit as the psoriasis lesions were usually healed. In addition, the spectral patterns varied significantly among the three measurements, which very likely demonstrate different representation of psoriasis at different depths within the skin.

At visit 1, an intensity decrease of the pronounced band intensity around 818 cm^{-1} and the 1080 cm^{-1} band in psoriasis can be observed compared to normal skin in depth-1 and -2. While the 818 cm^{-1} band could be related to δCCH alipathic, aromatic and olefinic vibrations of proteins, the 1080 cm^{-1} band is commonly associated to ν_{CC} skeletal vibrations of *gauche*-conformed lipids and PO_2 in nucleic acids and phospholipids. Similarly, in these depths, the psoriasis lesions show an increase of the 908 cm^{-1} band intensity, which is likely related to tyrosine [77]. At visit 2, this band is only weakly pronounced at depth-1. The 1460 cm^{-1} band intensity, likely related to $\delta(CH_2)(CH_3)$ vibrations of lipids and proteins, is decreased in psoriasis at depth-2 and especially at depth-3, where the overall intensity of this band is mostly pronounced. Shifts of Raman bands between psoriasis and normal skin were not observed. At visit 2, the differences between psoriasis and normal skin are not strongly pronounced.

The results of the classification from the leave-one-patient-out cross-validation are shown in Fig. 4. Thereby, the mean sensitivity of the prediction for each model built with different number of principal components (nPC) was calculated. This calculation was conducted for the results on the first and second visit separately. In particular, the two subplots give the results at the spectral (left) and patient (right) level, respectively. The patient-level prediction was obtained through a majority vote among the results from the five spectra of the same patient, i.e., the patient was assigned into the psoriasis group if 3 or more spectra were predicted as 'psoriasis'. The detailed results of the prediction are given in Table 1, at both spectral and patient-level. The numbers were summarized from the model using nPC=80. Again, the results from the two visits were presented separately. The mean sensitivity at visit 1 was approximately 71.7% and 87.5% at spectrum- and patient-level, respectively, which became 59.2% and 64.6% at visit 2. Noteworthy, we chose to report the results of nPC=80 because of the following fact. In Raman-based biological applications, the spectral-variations related to biological changes of interest are often extremely small and can easily be overwhelmed by other sources of variances. Therefore, the variances of interest are hardly presented in the first PCs. Using a large nPC helps to ensure all variances of interest are well considered in the modeling.

As was shown, the prediction performance decreased sharply at the second visit because the psoriasis lesions were healed in most cases. This could be explained, by the selection of the measurement positions at visit 1, which could clinically be clearly classified as psoriasis or normal skin. At visit 2, the majority of the lesions (73%) was clinically healed. The remaining lesions at visit 2 were either not healed yet, or could also be relapses of psoriasis lesions, which are known to often occur at the same sites [7,8]. In future studies, this could be controlled by more frequent visits including photo documentation of the healing progress of the lesions. However, the clinical diagnostic at visit 2 was considerably less obvious compared to visit 1, entailing a higher similarity between psoriasis and normal skin at the skin surface at visit 2. The discussed model features with 80 PCs a relative high model complexity. In order to evaluate if a model with less PCs can be used as well, we trained the PCA-LDA model with 18 PCs, which

Biomedical Optics EXPRESS

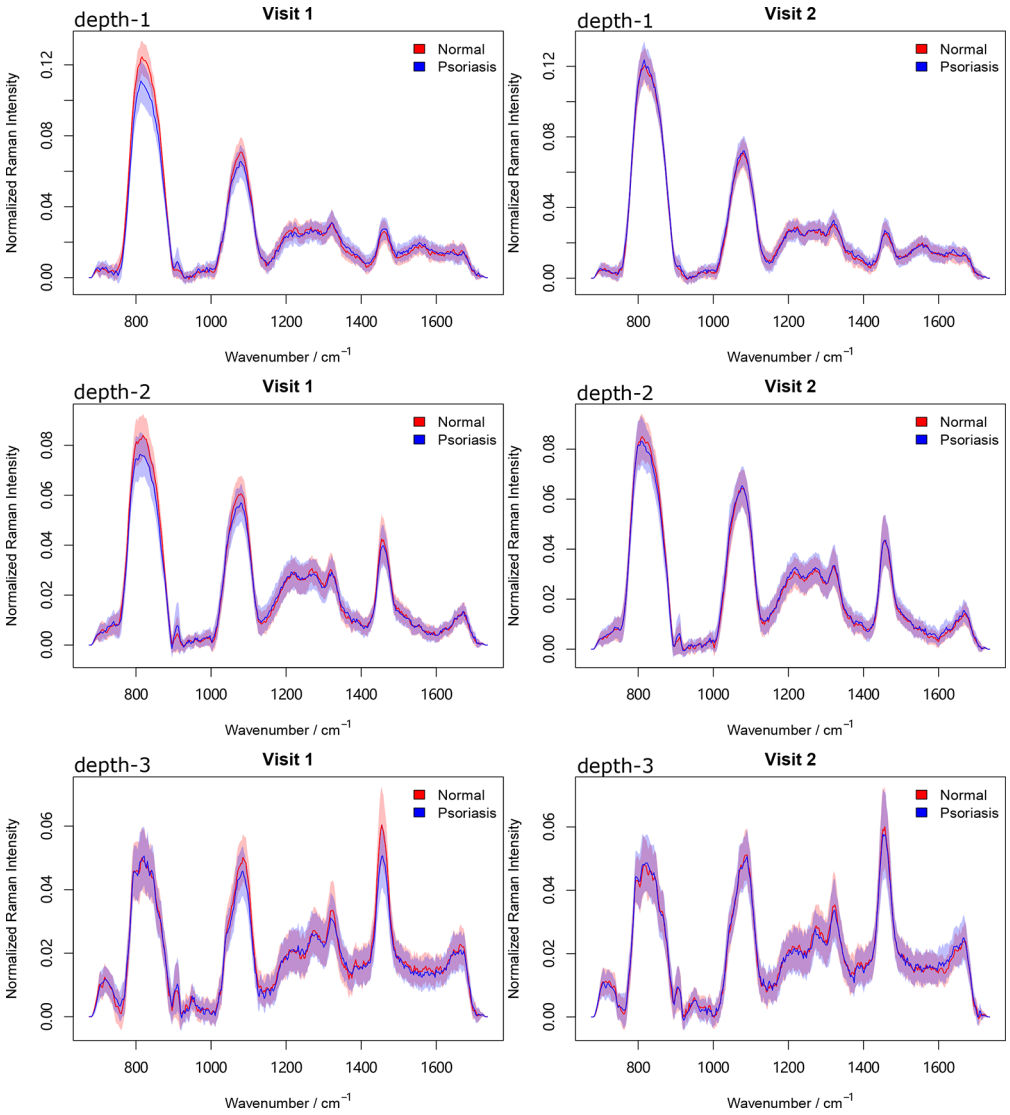

Fig. 3. Mean spectra of visit 1 (left column) and visit 2 (right column) for all patients measured from different depths within the skin (depth-1, -2, -3, respectively, where the first depth contains information from the most superficial skin areas and the third depth is related to the deepest skin areas).

Table 1. Results of prediction at spectral level (gray shade) and patient level with *nPC*=80. On both levels (spectra and patient) and for visit 1 and 2 a confusion table is shown, where the row corresponds to the reference diagnostics and the column represents the prediction. The results at patient level were obtained from a majority vote on the spectral level prediction.

			visit 1		visit 2	
			normal	psoriasis	normal	psoriasis
truth	spectral-level	normal	**89**	31	**96**	24
		psoriasis	37	**83**	74	**46**
	patient-level	normal	**23**	1	**22**	2
		psoriasis	5	**19**	15	**9**

Biomedical Optics EXPRESS

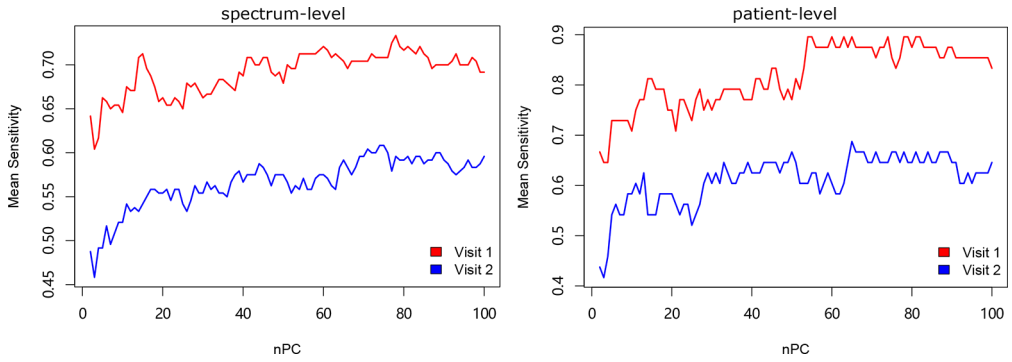

Fig. 4. Mean sensitivity at spectral level (left) and at patient level (right) in the cases of first and second visit. The mean sensitivity is scaled from 0 to 1, while 1 represents a perfect prediction. The mean sensitivities were calculated from the leave-one-patient-out cross-validation based on the models built with different number of principal components.

Table 2. Results of prediction at the spectral level (gray shade) and patient level with nPC=18. On both levels (spectra and patient) and for visit 1 and 2 a confusion table is shown, where the row corresponds to the reference diagnostics and the column represents the prediction. The results at the patient level were obtained from a majority vote on the spectral level prediction.

			visit 1		visit 2	
			normal	psoriasis	normal	psoriasis
truth	spectral-level	normal	**78**	42	**80**	40
		psoriasis	47	**73**	71	**49**
	patient-level	normal	**19**	5	**19**	5
		psoriasis	7	**17**	14	**10**

indicate the first peak of the first visit in Fig. 4. The corresponding evaluation results are given as a confusion table in Table 2. This model featured a patient-wise mean sensitivity of 73.42%, while the spectral-wise mean sensitivity was 63.19% at the first visit. At the second visit the mean sensitivity was 60.42% and 62.93% for patient and spectra, respectively. Both modelling results are a bit worse than the model with nPC=80.

Additionally, the mean sensitivity of the classification using the spectra measured from the three depths are separately shown in Figure S1. The sensitivities appeared to decrease with the depth. The decrease in prediction performance at the deeper skin layers (depth-2 and -3) can be explained by two facts, first of all are bio-spectroscopic signatures already contained in the depth-1 spectrum and secondly is the clinical diagnostics only performed on the superficial skin regions. One possibility to have a reference at the deeper skin layers and thereby improve the prediction at these depths could be, for instance, the utilization of *in vivo* laser scanning microscopy [11,12] at the identical skin positions measured with the fiber probe. Thereby, the sensitivity of the deeper skin layers could be achieved, independent from the clinical assessment of a dermatologist.

4. Conclusion

Currently, the efficiency of psoriasis treatment, its duration and termination is clinically controlled by a physician. However, clinically healthy skin can show psoriasis related alterations in the dermis, entailing a faster formation of relapses, if the treatment is terminated at this time. Thus, an objective criterion is required. The presented clinical study was performed on 24 patients with acute psoriasis lesions at the beginning of the treatment and four months later, when

Biomedical Optics EXPRESS

the psoriasis lesions were usually healed. The applied fiber probe based Raman spectroscopy using SORS-SERDS, was shown to have the potential to be used for the non-invasive *in vivo* determination of the treatment efficiency of psoriasis, in order to prevent the faster occurrence of relapses in case of a too short treatment. On the patient level, a mean sensitivity of ≥85% was achieved at visit 1, where the measurement positions were classified based on the clinical appearance. At visit 2, the sensitivity decreased to ≈65%, due to the varying healing process. The presented study shows the potential of the SORS-SERDS method for the non-invasive *in vivo* determination of the treatment efficiency of psoriasis. Further studies need to investigate a direct correlation of the SORS-SERDS data with direct measurements of the inflamed lesions within the skin, the investigations of different states of psoriasis lesions and their SORS-SERDS characteristics and the long-term patient outcome if treatment is monitored using SORS-SERDS. These studies will lead to a SORS-SERDS tool to better determine the treatment efficiency of psoriasis, which finally help patients.

Funding. China Scholarship Council; Bundesministerium für Bildung und Forschung (13N13245); Seventh Framework Programme of the European Union (PhotoSkin).

Acknowledgments. The contributions of Iwan Schie and the dermatologists Alexa Patzelt and Sora Jung are highly appreciated. We acknowledge support from the German Research Foundation (DFG) and the Open Access Publication Fund of Charité – Universitätsmedizin Berlin.

Disclosures. The authors declare no conflicts of interest.

Supplemental document. See Supplement 1 for supporting content.

References

1. C. E. M. Griffiths and J. N. W. N. Barker, "Pathogenesis and clinical features of psoriasis," The Lancet **370**(9583), 263–271 (2007).
2. E. Ogawa, Y. Sato, A. Minagawa, and R. Okuyama, "Pathogenesis of psoriasis and development of treatment," J. Dermatol. **45**(3), 264–272 (2018).
3. L. Naldi, "Epidemiology of psoriasis," Curr Drug Targets Inflamm Allergy **3**(2), 121–128 (2004).
4. G. Krueger, J. Koo, M. Lebwohl, A. Menter, R. S. Stern, and T. Rolstad, "The impact of psoriasis on quality of life: results of a 1998 National Psoriasis Foundation patient-membership survey," Arch Dermatol. **137**, 280–284 (2001).
5. F. Sampogna, F. Sera, and D. Abeni, "Measures of clinical severity, quality of life, and psychological distress in patients with psoriasis: a cluster analysis," J. Invest Dermatol. **122**(3), 602–607 (2004).
6. M. Goodfield, S. M. Hull, D. Holland, G. Roberts, E. Wood, S. Reid, and W. Cunliffe, "Investigations of the 'active' edge of plaque psoriasis: vascular proliferation precedes changes in epidermal keratin," Br. J. Dermatol. **131**(6), 808–813 (1994).
7. R. A. Clark, "Gone but not forgotten: lesional memory in psoriatic skin," J. Invest Dermatol. **131**(2), 283–285 (2011).
8. M. Suarez-Farinas, J. Fuentes-Duculan, M. A. Lowes, and J. G. Krueger, "Resolved psoriasis lesions retain expression of a subset of disease-related genes," J. Invest Dermatol. **131**(2), 391–400 (2011).
9. F. Chamian, M. A. Lowes, S. L. Lin, E. Lee, T. Kikuchi, P. Gilleaudeau, M. Sullivan-Whalen, I. Cardinale, A. Khatcherian, I. Novitskaya, K. M. Wittkowski, and J. G. Krueger, "Alefacept reduces infiltrating T cells, activated dendritic cells, and inflammatory genes in psoriasis vulgaris," Proc. Natl. Acad. Sci. U. S. A. **102**(6), 2075–2080 (2005).
10. L. C. Zaba, I. Cardinale, P. Gilleaudeau, M. Sullivan-Whalen, M. Suarez-Farinas, J. Fuentes-Duculan, I. Novitskaya, A. Khatcherian, M. J. Bluth, M. A. Lowes, and J. G. Krueger, "Amelioration of epidermal hyperplasia by TNF inhibition is associated with reduced Th17 responses," J. Exp. Med. **204**(13), 3183–3194 (2007).
11. R. Archid, A. Patzelt, B. Lange-Asschenfeldt, S. S. Ahmad, M. Ulrich, E. Stockfleth, S. Philipp, W. Sterry, and J. Lademann, "Confocal laser-scanning microscopy of capillaries in normal and psoriatic skin," J. Biomed. Opt. **17**(10), 101511 (2012).
12. R. Archid, H. P. Duerr, A. Patzelt, S. Philipp, H. J. Rowert-Huber, M. Ulrich, M. C. Meinke, F. Knorr, and J. Lademann, "Relationship between Histological and Clinical Course of Psoriasis: A Pilot Investigation by Reflectance Confocal Microscopy during Goeckerman Treatment," Skin Pharmacol. Physiol. **29**(1), 47–54 (2016).
13. M. Egawa, N. Kunizawa, T. Hirao, T. Yamamoto, K. Sakamoto, T. Terui, and H. Tagami, "In vivo characterization of the structure and components of lesional psoriatic skin from the observation with Raman spectroscopy and optical coherence tomography: a pilot study," J. Dermatol. Sci. **57**(1), 66–69 (2010).
14. A. Pietrzak, A. Michalak-Stoma, G. Chodorowska, and J. C. Szepietowski, "Lipid disturbances in psoriasis: an update," Mediators Inflamm 2010 (2010).
15. E. Proksch, "The role of emollients in the management of diseases with chronic dry skin," Skin Pharmacol. Physiol. **21**(2), 75–80 (2008).

Biomedical Optics EXPRESS

16. T. Meyer, R. Ackermann, R. Kammel, M. Schmitt, S. Nolte, A. Tünnermann, and J. Popp, "CARS-imaging guidance for fs-laser ablation precision surgery," Analyst **144**(24), 7310–7317 (2019).
17. M. Weinigel, H. G. Breunig, M. Kellner-Höfer, R. Bückle, M. E. Darvin, M. Klemp, J. Lademann, and K. König, "In vivohistology: optical biopsies with chemical contrast using clinical multiphoton/coherent anti-Stokes Raman scattering tomography," Laser Phys. Lett. **11**(5), 055601 (2014).
18. J. Schleusener, P. Gluszczynska, C. Reble, I. Gersonde, J. Helfmann, J. W. Fluhr, J. Lademann, J. Röwert-Huber, A. Patzelt, and M. C. Meinke, "In vivo study for the discrimination of cancerous and normal skin using fibre probe-based Raman spectroscopy," Exp. Dermatol. **24**(10), 767–772 (2015).
19. M. Gniadecka, H. C. Wulf, O. F. Nielsen, D. H. Christensen, and J. Hercogova, "Distinctive molecular abnormalities in benign and malignant skin lesions: studies by Raman spectroscopy," Photochem. Photobiol. **66**(4), 418–423 (1997).
20. H. Lui, J. Zhao, D. McLean, and H. Zeng, "Real-time Raman spectroscopy for in vivo skin cancer diagnosis," Cancer Res. **72**(10), 2491–2500 (2012).
21. C. A. Lieber, S. K. Majumder, D. L. Ellis, D. D. Billheimer, and A. Mahadevan-Jansen, "In vivo nonmelanoma skin cancer diagnosis using Raman microspectroscopy," Lasers Surg. Med. **40**(7), 461–467 (2008).
22. M. Larraona-Puy, A. Ghita, A. Zoladek, W. Perkins, S. Varma, I. H. Leach, A. A. Koloydenko, H. Williams, and I. Notingher, "Development of Raman microspectroscopy for automated detection and imaging of basal cell carcinoma," J. Biomed. Opt. **14**(5), 054031 (2009).
23. A. Nijssen, T. C. Bakker Schut, F. Heule, P. J. Caspers, D. P. Hayes, M. H. A. Neumann, and G. J. Puppels, "Discriminating basal cell carcinoma from its surrounding tissue by Raman spectroscopy," J. Investigative Dermatol. **119**(1), 64–69 (2002).
24. T. Bocklitz, M. Putsche, C. Stüber, J. Käs, A. Niendorf, P. Rösch, and J. Popp, "A comprehensive study of classification methods for medical diagnosis," J. Raman Spectrosc. **40**(12), 1759–1765 (2009).
25. M. Hedegaard, C. Krafft, H. J. Ditzel, L. E. Johansen, S. Hassing, and J. Popp, "Discriminating isogenic cancer cells and identifying altered unsaturated fatty acid content as associated with metastasis status, using k-means clustering and partial least squares-discriminant analysis of Raman maps," Anal. Chem. **82**(7), 2797–2802 (2010).
26. P. D. Pudney, E. Y. Bonnist, P. J. Caspers, J. P. Gorce, C. Marriot, G. J. Puppels, S. Singleton, and M. J. van der Wolf, "A new in vivo Raman probe for enhanced applicability to the body," Appl. Spectrosc. **66**(8), 882–891 (2012).
27. C. Choe, J. Lademann, and M. E. Darvin, "A depth-dependent profile of the lipid conformation and lateral packing order of the stratum corneum in vivo measured using Raman microscopy," Analyst **141**(6), 1981–1987 (2016).
28. C. Choe, J. Schleusener, J. Lademann, and M. E. Darvin, "Keratin-water-NMF interaction as a three layer model in the human stratum corneum using in vivo confocal Raman microscopy," Sci. Rep. **7**(1), 15900 (2017).
29. C. Choe, J. Lademann, and M. E. Darvin, "Depth profiles of hydrogen bound water molecule types and their relation to lipid and protein interaction in the human stratum corneum in vivo," Analyst **141**(22), 6329–6337 (2016).
30. J. S. Ri, S. H. Choe, J. Schleusener, J. Lademann, C. S. Choe, and M. E. Darvin, "In vivo Tracking of DNA for Precise Determination of the Stratum Corneum Thickness and Superficial Microbiome Using Confocal Raman Microscopy," Skin Pharmacol Physiol. **33**(1), 30–37 (2020).
31. M. E. Darvin, I. Gersonde, M. Meinke, W. Sterry, and J. Lademann, "Non-invasive in vivo determination of the carotenoids beta-carotene and lycopene concentrations in the human skin using the Raman spectroscopic method," J. Phys. D: Appl. Phys. **38**(15), 2696–2700 (2005).
32. C. Choe, J. Ri, J. Schleusener, J. Lademann, and M. E. Darvin, "The non-homogenous distribution and aggregation of carotenoids in the stratum corneum correlates with the organization of intercellular lipids in vivo," Exp. Dermatol. **28**(11), 1237–1243 (2019).
33. M. E. Darvin, J. Schleusener, F. Parenz, O. Seidel, C. Krafft, J. Popp, and J. Lademann, "Confocal Raman microscopy combined with optical clearing for identification of inks in multicolored tattooed skin in vivo," Analyst **143**(20), 4990–4999 (2018).
34. J. Schleusener, J. Lademann, and M. E. Darvin, "Depth-dependent autofluorescence photobleaching using 325, 473, 633, and 785 nm of porcine ear skin ex vivo," J. Biomed. Opt. **22**(9), 091503 (2017).
35. A. Y. Sdobnov, V. Tuchin, J. Lademann, and M. E. Darvin, "Confocal Raman microscopy supported by optical clearing treatment of the skin—influence on collagen hydration," J. Phys. D: Appl. Phys. **50**(28), 285401 (2017).
36. J. Wohlrab, A. Vollmann, S. Wartewig, W. C. Marsch, and R. Neubert, "Noninvasive characterization of human stratum corneum of undiseased skin of patients with atopic dermatitis and psoriasis as studied by Fourier transform Raman spectroscopy," Biopolymers **62**(3), 141–146 (2001).
37. G. Zhang, D. J. Moore, R. Mendelsohn, and C. R. Flach, "Vibrational Microspectroscopy and Imaging of Molecular Composition and Structure During Human Corneocyte Maturation," J. Invest. Dermatol. **126**(5), 1088–1094 (2006).
38. H. G. M. Edwards, A. C. Williams, and B. W. Barry, "Potential applications of FT-Raman spectroscopy for dermatological diagnostics," J. Mol. Struct. **347**, 379–387 (1995).
39. G. Bernard, M. Auger, J. Soucy, and R. Pouliot, "Physical characterization of the stratum corneum of an in vitro psoriatic skin model by ATR-FTIR and Raman spectroscopies," Biochim Biophys Acta. **1770**(9), 1317–1323 (2007).
40. C. Choe, J. Lademann, and M. E. Darvin, "Lipid organization and stratum corneum thickness determined in vivo in human skin analyzing lipid–keratin peak (2820–3030 cm−1) using confocal Raman microscopy," J. Raman Spectrosc. **47**(11), 1327–1331 (2016).

Biomedical Optics EXPRESS

41. M. Osada, M. Gniadecka, and H. C. Wulf, "Near-infrared Fourier transform Raman spectroscopic analysis of proteins, water and lipids in intact normal stratum corneum and psoriasis scales," Exp. Dermatol. **13**(6), 391–395 (2004).
42. P. J. Caspers, G. W. Lucassen, E. A. Carter, H. A. Bruining, and G. J. Puppels, "In vivo confocal Raman microspectroscopy of the skin: noninvasive determination of molecular concentration profiles," J. Investigative Dermatol. **116**(3), 434–442 (2001).
43. U. Utzinger and R. R. Richards-Kortum, "Fiber optic probes for biomedical optical spectroscopy," J. Biomed. Opt. **8**(1), 121–147 (2003).
44. I. Latka, S. Dochow, C. Krafft, B. Dietzek, and J. Popp, "Fiber optic probes for linear and nonlinear Raman applications – Current trends and future development," Laser Photonics Rev. **7**(5), 698–731 (2013).
45. Z. Huang, H. Zeng, I. Hamzavi, D. I. McLean, and H. Lui, "Rapid near-infrared Raman spectroscopy system for real-time in vivo skin measurements," Opt. Lett. **26**(22), 1782–1784 (2001).
46. A. A. P. Boechat, D. Su, D. R. Hall, and J. D. C. Jones, "Bend loss in large core multimode optical fiber beam delivery systems," Appl. Opt. **30**(3), 321–327 (1991).
47. C. Reble, I. Gersonde, C. A. Lieber, and J. Helfmann, "Influence of tissue absorption and scattering on the depth dependent sensitivity of Raman fiber probes investigated by Monte Carlo simulations," Biomed. Opt. Express **2**(3), 520–533 (2011).
48. P. Matousek, I. P. Clark, E. R. C. Draper, M. D. Morris, A. E. Goodship, N. Everall, M. Towrie, W. F. Finney, and A. W. Parker, "Subsurface probing in diffusely scattering media using spatially offset Raman spectroscopy," Appl. Spectrosc. **59**(4), 393–400 (2005).
49. S. Mosca, P. Dey, M. Salimi, F. Palombo, N. Stone, and P. Matousek, "Non-invasive depth determination of inclusion in biological tissues using spatially offset Raman spectroscopy with external calibration," Analyst (2020).
50. A. Nijssen, K. Maquelin, L. F. Santos, P. J. Caspers, T. C. Bakker Schut, J. C. den Hollander, M. H. A. Neumann, and G. J. Puppels, "Discriminating basal cell carcinoma from perilesional skin using high wave-number Raman spectroscopy," J. Biomed. Opt. **12**(3), 034004 (2007).
51. J. T. Motz, M. Hunter, L. H. Galindo, J. A. Gardecki, J. R. Kramer, R. R. Dasari, and M. S. Feld, "Optical fiber probe for biomedical Raman spectroscopy," Appl. Opt. **43**(3), 542–554 (2004).
52. R. Richards-Kortum and E. Sevick-Muraca, "Quantitative optical spectroscopy for tissue diagnosis," Annu. Rev. Phys. Chem. **47**(1), 555–606 (1996).
53. E. G. Borisova, L. P. Angelova, and E. P. Pavlova, "Endogenous and Exogenous Fluorescence Skin Cancer Diagnostics for Clinical Applications," IEEE J. Sel. Top. Quantum Electron. **20**(2), 211–222 (2014).
54. A. A. Stratonnikov, V. S. Polikarpov, and V. B. Loschenov, "Photobleaching of endogenous fluorochroms in tissues in vivo during laser irradiation," Proc. SPIE **4241**, 13–24 (2001).
55. Z. Huang, H. Zeng, I. Hamzavi, A. Alajlan, E. Tan, D. I. McLean, and H. Lui, "Cutaneous melanin exhibiting fluorescence emission under near-infrared light excitation," J. Biomed. Opt. **11**(3), 034010 (2006).
56. X. Han, H. Lui, D. I. McLean, and H. Zeng, "Near-infrared autofluorescence imaging of cutaneous melanins and human skin in vivo," J. Biomed. Opt. **14**(2), 024017 (2009).
57. B. P. Yakimov, E. A. Shirshin, J. Schleusener, A. S. Allenova, V. V. Fadeev, and M. E. Darvin, "Melanin distribution from the dermal–epidermal junction to the stratum corneum: non-invasive in vivo assessment by fluorescence and Raman microspectroscopy," Sci. Rep. **10**(1), 14374 (2020).
58. S. Koljenovic, T. C. Bakker Schut, R. Wolthuis, B. de Jong, L. Santos, P. J. Caspers, J. M. Kros, and G. J. Puppels, "Tissue characterization using high wave number Raman spectroscopy," J. Biomed. Opt. **10**(3), 031116 (2005).
59. F. Knorr, Z. J. Smith, and S. Wachsmann-Hogiu, "Development of a time-gated system for Raman spectroscopy of biological samples," Opt. Express **18**(19), 20049–20058 (2010).
60. R. Adami and J. Kiefer, "Light-emitting diode based shifted-excitation Raman difference spectroscopy (LED-SERDS)," Analyst **138**(21), 6258–6261 (2013).
61. B. B. Praveen, P. C. Ashok, M. Mazilu, A. Riches, S. Herrington, and K. Dholakia, "Fluorescence suppression using wavelength modulated Raman spectroscopy in fiber-probe-based tissue analysis," J. Biomed. Opt. **17**(7), 0770061 (2012).
62. A. C. De Luca, M. Mazilu, A. Riches, C. S. Herrington, and K. Dholakia, "Online fluorescence suppression in modulated Raman spectroscopy," Anal. Chem. **82**(2), 738–745 (2010).
63. S. Brustlein, P. Berto, R. Hostein, P. Ferrand, C. Billaudeau, D. Marguet, A. Muir, J. Knight, and H. Rigneault, "Double-clad hollow core photonic crystal fiber for coherent Raman endoscope," Opt. Express **19**(13), 12562 (2011).
64. K. M. Tan, G. P. Singh, C. S. Herrington, and C. T. A. Brown, "Near-infrared Raman spectroscopy using hollow-core photonic bandgap fibers," Opt. Commun. **283**(16), 3204–3206 (2010).
65. M. Kasha, "Characterization of electronic transitions in complex molecules," Discuss. Faraday Soc. **9**, 14–19 (1950).
66. N. D. Magee, J. S. Villaumie, E. T. Marple, M. Ennis, J. S. Elborn, and J. J. McGarvey, "Ex vivo diagnosis of lung cancer using a Raman miniprobe," J. Phys. Chem. B **113**(23), 8137–8141 (2009).
67. M. Braune, M. Maiwald, M. E. Darvin, B. Eppich, B. Sumpf, J. Lademann, and G. Trankle, "Shifted excitation resonance Raman difference spectroscopy system suitable for the quantitative in vivo detection of carotenoids in human skin," Laser Phys. Lett. **15**(11), 115601 (2018).
68. K. Sowoidnich, M. Towrie, M. Maiwald, B. Sumpf, and P. Matousek, "Shifted excitation raman difference spectroscopy with charge-shifting charge-coupled device (CCD) lock-in detection," Appl. Spectrosc. **73**, 000370281985935 (2019).

Biomedical Optics EXPRESS

69. T. B. Fitzpatrick, "The validity and practicality of sun-reactive skin types I through VI," Arch Dermatol. **124**(6), 869–871 (1988).
70. L. Wang, S. L. Jacques, and L. Zheng, "MCML—Monte Carlo modeling of light transport in multi-layered tissues," Comput. Methods and Programs Biomed. **47**(2), 131–146 (1995).
71. R Core Team, R Foundation for Statistical Computing, Vienna, Austria, 2013.
72. T. W. Bocklitz, S. Guo, O. Ryabchykov, N. Vogler, and J. Popp, "Raman based molecular imaging and analytics: a magic bullet for biomedical applications!?" Analytical chemistry (2015).
73. T. Bocklitz, T. Dörfer, R. Heinke, M. Schmitt, and J. Popp, "Spectrometer calibration protocol for Raman spectra recorded with different excitation wavelengths," Spectrochim. Acta, Part A **149**, 544–549 (2015).
74. S. Guo, O. Chernavskaia, J. Popp, and T. Bocklitz, "Spectral reconstruction for shifted-excitation Raman difference spectroscopy (SERDS)," Talanta **186**, 372–380 (2018).
75. C. Ryan, E. Clayton, W. Griffin, S. Sie, and D. Cousens, "SNIP, a statistics-sensitive background treatment for the quantitative analysis of PIXE spectra in geoscience applications," Nucl. Instrum. Methods Phys. Res., Sect. B **34**(3), 396–402 (1988).
76. W. N. Venables and B. D. Ripley, *Modern Applied Statistics with S*, 4 ed., Statistics and Computing (Springer, 2002).
77. A. C. S. Talari, Z. Movasaghi, S. Rehman, and I. U. Rehman, "Raman spectroscopy of biological tissues," Appl. Spectrosc. Rev. **50**(1), 46–111 (2015).